Available online at www.sciencedirect.com
SCIENCE DIRECT®
Precision Engineering 28 (2004) 152–163
PRECISION ENGINEERING
www.elsevier.com/locate/precision

Optical 3D profilometer for in-process measurement of microsurface based on phase retrieval technique

Atsushi Taguchi*, Takashi Miyoshi, Yasuhiro Takaya, Satoru Takahashi[1]

Department of Mechanical Engineering and Systems, Osaka University, Suita, Osaka 565-0871, Japan

Received 3 March 2003; received in revised form 9 July 2003; accepted 25 July 2003

Abstract

We have proposed an optical method that can be applied to in-process or in situ measurement of the microsurface profile. The present method is based on optically performed spectral analysis and the phase retrieval technique. Spectral information of a surface profile is obtained by measuring the Fraunhofer diffraction intensity. The phase retrieval technique is used to reconstruct the surface profile from the measured spectrum. We have developed an instrument on the basis of the general principles of the present method, and measured the surface of a reference standard having rectangular pockets 44 nm deep at intervals of 10 μm. The measured surface profile was in good agreement with the nominal dimensions of the specimen as well as the surface profile obtained by atomic force microscopy (AFM).

PACS: 07.60.-j; 42.30.Rx; 42.25.Fx; 68.35.Bs; 81.70.Fy

Keywords: Optical profiler; Phase retrieval; Diffraction intensity; Scattering; Microsurface profile; In-process measurement

1. Introduction

With the advance of microtechnology, ever-improving metrology is required for the production of precision-engineered microparts. Precise systems such as microelectromechanical systems (MEMS) and micro-optical devices incorporate assemblies of microparts having a size on the order of a few to a few hundred micrometers [1], and tolerances of geometric dimensions of the individual microparts must be controlled to an accuracy of less than sub-micrometer order. While measurement techniques such as scanning probe microscopy (SPM) and interferometry are currently used to acquire dimensional characteristics of engineered microsurfaces [2], methods for in situ or in-process measurement is increasingly required in the microparts industry.

Here we describe an optical measurement method that can be applied to the in-process measurement of microsurface profiles. In the present method, spectral information of a surface profile is obtained by measuring the Fraunhofer diffraction intensity. The surface profile is then reconstructed from the measured spectrum by the phase retrieval technique [3–5]. The present method offers the following advantages for in-process measurements. A surface profile within the whole illuminated area can be measured simultaneously and no scanning process is imposed. A long working distance is achievable with no contact with the work surface. Required time for data acquisition is short. Measurements of the diffraction intensity are not likely to be affected by the vibration of work surface.

One noteworthy feature of the present method is the ability to obtain a deterministic profile of the measured surface from the diffraction intensity. Although diffraction is known to be a useful phenomenon for surface studies and characterizations, most efforts have been devoted to obtaining area-averaged statistical properties of diffracting structures, such as roughness parameters [6–9]. One reason is ascribed to the difficulty of determining the phase of the diffraction field. Recently, an apparatus for directly measuring the phase of the diffraction field was proposed by Destouches et al. and applied to the surface reconstruction [10]. However, in-process implementation of this technique is not straightforward. Meanwhile, we previously proposed the basic idea of using the phase retrieval technique for deterministic profile reconstruction from the diffraction intensity [11], and the iterative phase retrieval algorithm of Fienup type [5,12,13] was adopted in our recent work [14]. This report is based on the continuous improvements and developments in our present work.

* Corresponding author. Tel.: +81-6-6879-7321; fax: +81-6-6879-7320.
E-mail address: taguchi@optim.mech.eng.osaka-u.ac.jp (A. Taguchi).
[1] Present address: Department of Precision Engineering, The University of Tokyo, Hongo, Bunkyo-ku, Tokyo 113-8656, Japan.

0141-6359/$ – see front matter © 2003 Elsevier Inc. All rights reserved.
doi:10.1016/j.precisioneng.2003.07.002

In what follows, the general principles of the proposed method is described in Section 2. Sections 3 and 4 are dedicated to describing the basic concept of the instrument design and the optical instrumentation. The resolution, sampling requirements, and illumination conditions are also described. The experimental results and discussions are presented in Section 5.

2. Principle of measurement

2.1. Spectral analysis of surface profile and synthesis

An object having the surface profile $h(x, y)$ is located in object plane Π, as shown in Fig. 1. The object surface is coherently illuminated by a plane monochromatic wave incident normal to plane Π. The complex amplitude of the scattering light from the surface (we will refer to this as object wave here) is expressed as

$$V(x, y) = |V(x, y)|\exp[i\theta(x, y)], \tag{1}$$

where

$$\theta(x, y) = \frac{4\pi}{\lambda}h(x, y), \tag{2}$$

is the phase difference brought into by the height irregularities in the surface, and λ is the wavelength of the incident radiation used.

The object wave gives rise to a Fraunhofer pattern in the lens focal plane Γ, which greatly depends on the phase of the object wave. By the Fraunhofer formula, the diffraction field $U(X, Y)$ at the spatial coordinates (X, Y) in plane Γ is given as

$$U(X, Y) = \iint_D V(x, y)\exp\left[-i\frac{2\pi}{\lambda}\left(\frac{X}{f}x + \frac{Y}{f}y\right)\right] dx\,dy, \tag{3}$$

where f is the distance to focal plane Γ from the lens, and the integration is taken over the area D of object plane Π covered by the illuminated area on the surface [15]. Standardizing the spatial coordinates (X, Y) by the product of the lens focal length f and the wavelength λ, we obtain $|U(p, q)|^2 = |U(X/\lambda f, Y/\lambda f)|^2$, a mapping of the power spectrum density (PSD) of the object wave, from the measured diffraction intensity $I(X, Y) = |U(X, Y)|^2$. The information of the surface profile is recorded in the form of the spectral intensity at the corresponding spatial frequency in the spatial frequency domain.

Fig. 2 shows a schema of surface profile reconstruction from the PSD of the object wave. The PSD provided from the measured diffraction intensity is a second-order information, while the object wave is fully characterized by its complete Fourier spectrum that is in general a complex-valued function. The lack of information is supplemented by measuring the intensity of the object wave (object intensity) $i(x, y) = |V(x, y)|^2$. With the pair of intensity data measured in both the spatial and spatial frequency domains, phase retrieval allows us to determine the phase of the object wave. The sur-

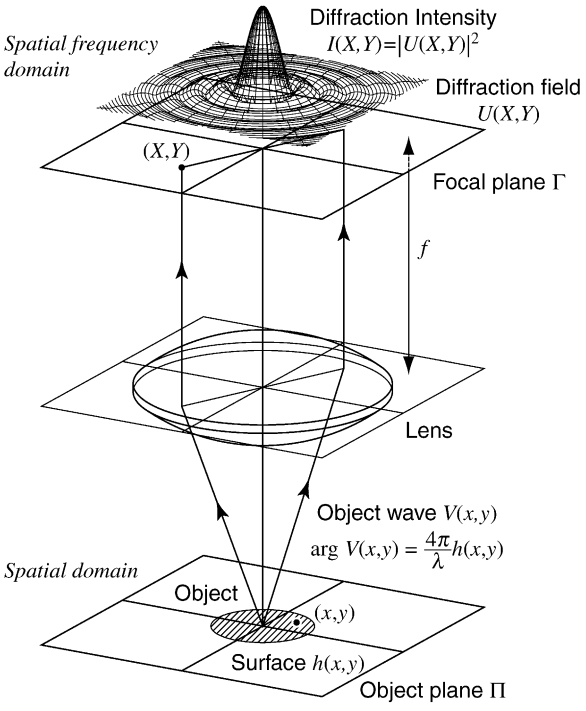

Fig. 1. Schematic of optical system for obtaining Fraunhofer diffraction. The power spectrum of the object wave can be obtained by measuring diffraction intensity. f, focal length of the lens.

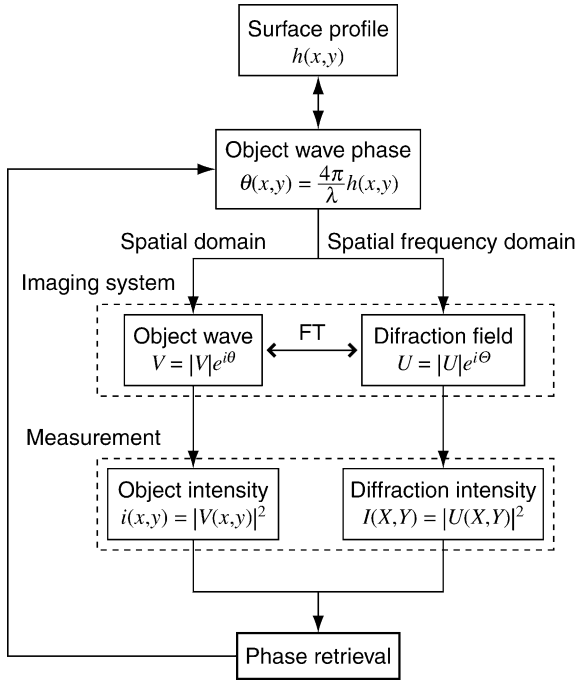

Fig. 2. Schema of surface reconstruction. Surface profile, or equivalently, the phase of the object wave is determined from two intensity data: diffraction intensity in the spatial frequency domain and object intensity in the spatial domain. Phase retrieval technique is used for the phase determination. FT, Fourier transform.

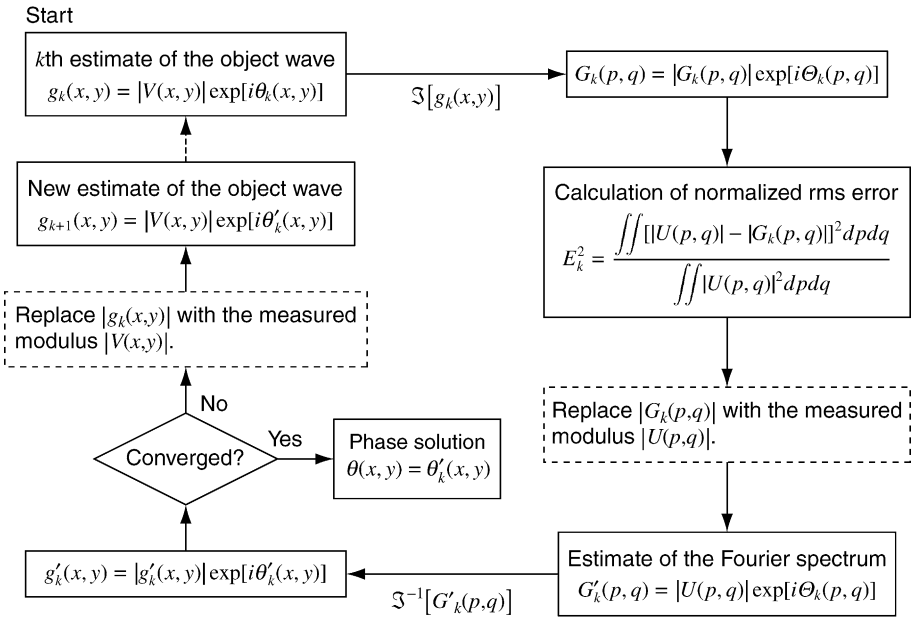

Fig. 3. Block diagram of the phase retrieval algorithm. The convergence of the algorithm is monitored by calculating the normalized rms error E_k^2. $\Im$ and $\Im^{-1}$ are the Fourier transform operator and its inverse, respectively.

face profile is calculated from the determined phase using Eq. (2).

2.2. Phase retrieval algorithm

A block diagram of the phase retrieval algorithm [4,5] is shown in Fig. 3. The algorithm involves iterative Fourier transform back and forth between the spatial and spatial frequency domains and the application of the measured intensity data in each domain. Denoting an estimate of the phase for the kth iteration as $\theta_k(x, y)$, the estimate of the object wave $g_k(x, y)$ is expressed as $g_k(x, y) = |V(x, y)|\exp[i\theta_k(x, y)]$. The following four steps are applied iteratively to this estimate, $g_k(x, y)$: (1) Fourier transform the estimate of the object wave; (2) replace the modulus of the resulting Fourier transform with the measured Fourier modulus to form an estimate of the Fourier spectrum; (3) inverse Fourier transform the estimate of the Fourier spectrum; and (4) replace the modulus of the resulting function with the measured modulus to form a new estimate of the object wave. This is described by

$$G_k(p, q) = |G_k(p, q)|\exp[i\Theta_k(p, q)] = \Im[g_k(x, y)], \quad (4)$$

$$G'_k(p, q) = |U(p, q)|\exp[i\Theta_k(p, q)], \quad (5)$$

$$g'_k(x, y) = |g'_k(x, y)|\exp[i\theta'_k(x, y)] = \Im^{-1}[G'_k(p, q)], \quad (6)$$

$$g_{k+1}(x, y) = |V(x, y)|\exp[i\theta_{k+1}(x, y)] = |V(x, y)|\exp[i\theta'_k(x, y)], \quad (7)$$

where $G_k(p, q)$ and $\Theta_k(p, q)$ are the estimate of the Fourier spectrum and its phase, and $\Im$ and $\Im^{-1}$ are the Fourier transform operator and its inverse, respectively.

The convergence of the algorithm is monitored by calculating the normalized rms error, E_k^2, defined in the spatial frequency domain, by

$$E_k^2 = \frac{\iint[|U(p, q)| - |G_k(p, q)|]^2 dp\, dq}{\iint |U(p, q)|^2 dp\, dq}. \quad (8)$$

The value of rms error E_k^2 decreases at each iteration [4]. The iterations continue until the value of error E_k^2 converges to be sufficiently equal to zero or remains unchanged with a number of further iterations. When the error E_k^2 reaches a minimum, a solution has been found. Note that the solution is known to be almost always unique, except for minor ambiguities such as rotations by $2/\pi$, linear shifts, and multiplication by a unit magnitude complex constant [3].

In order to lessen the computation time required as well as to remove the minor ambiguities in the phase solution, it is desirable to make an educated guess at the correct phase distribution as the initial estimate of the algorithm. Indeed, we are concerned here with engineering surfaces, which are usually processed according to the designed geometrical quantities such as dimensions or size parameters. Such a priori knowledge about the engineering surface should be used as the initial estimate of the iterative algorithm.

3. Instrument design

3.1. Imaging system

A conceptual diagram of the imaging system for measuring the required two intensities is shown in Fig. 4. Because it is very important to obtain the power spectrum of an object

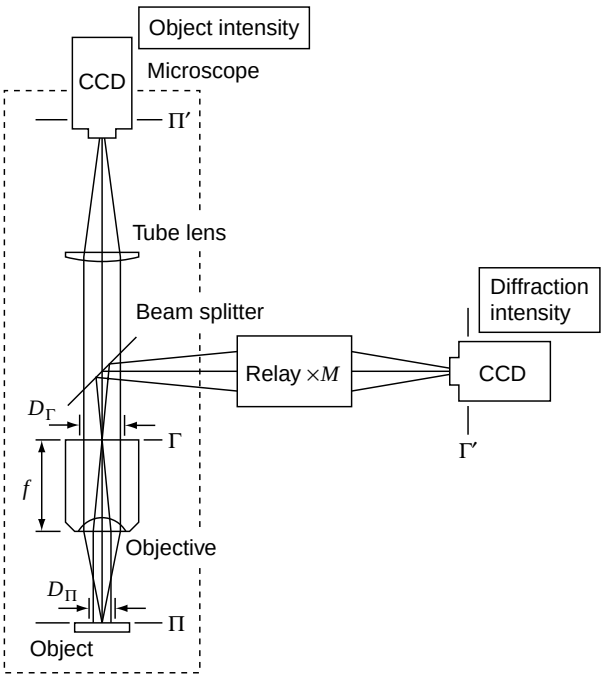

Fig. 4. Conceptual diagram illustrating an imaging system for measuring two intensities. Object intensity in plane Π is measured using the configuration of the optical microscopy, while diffraction field appearing in the objective back focal plane Γ is relayed onto its conjugate plane Γ'. Π' is the image plane of the microscope. f, focal length of the objective. M, magnification of the relay optics.

wave at correctly corresponding spatial frequencies, an objective is used for the transforming lens. Plane Γ, the objective back focal plane in which the diffraction field appears, exists inside the barrel of the objective. We use relay optics so that the diffraction intensity is measured on the conjugate plane Γ'. On the other hand, the object intensity is measured by the configuration of an optical microscope consisting of an objective and a tube lens. Because a beam splitter is inserted in the optical path, an infinity-corrected optical microscope is a suitable choice.

3.1.1. Lateral resolution

The lateral resolution in the present method is limited by the bandwidth of the spectrum measured. Assuming that the imaging system is shift invariant and obeys the sine condition, the bandwidth of the spectrum depends on the objective numerical aperture (NA) and the wavelength λ, in accordance with the formula [15]

$$p^2 + q^2 \leq \left(\frac{\mathrm{NA}}{\lambda}\right)^2. \tag{9}$$

The maximum spatial frequency that can be measured by the system is NA/λ. Thus, the period, Δ, of the finest sinusoidal phase distribution resolvable in the spatial domain is

$$\Delta = \frac{\lambda}{\mathrm{NA}}. \tag{10}$$

We use the value of Δ given by Eq. (10) as a theoretical criterion of the lateral resolution.

3.1.2. Sampling

The pixel format of CCDs required for properly sampling each intensity data is derived from the size of intensity images and the sampling theorem. First, we discuss the pixel format required for the measurement of diffraction intensity. Letting D_Γ and f be the diameter of the diffraction field in the back focal plane Γ and the focal length of the objective, respectively (see Fig. 4), D_Γ is given by Eq. (9) as $D_\Gamma = 2f \times \mathrm{NA}$. This is magnified M-fold by the relay optics and then, $D_{\Gamma'}$, the size of the diffraction field in the image plane Γ' is given by

$$D_{\Gamma'} = 2Mf \times \mathrm{NA}. \tag{11}$$

For obtaining high-frequency components up to the upper limit of the bandwidth, the device size of the CCD must be larger than the value of $D_{\Gamma'}$. On the other hand, the sampling interval of the diffraction intensity is given according to the frequency sampling theorem [16]. When the object wave has the extent D_Π in object plane Π, the spectrum of the object wave must be sampled with an interval of less than $1/D_\Pi$ in the spatial frequency domain, which corresponds to the interval of $\lambda f/D_\Pi$ in plane Γ. Thus, in image plane Γ', the diffraction intensity is required to be sampled with the maximum interval of

$$\Delta D_{\Gamma'} = M \times \frac{\lambda f}{D_\Pi}. \tag{12}$$

For the measurement of the object intensity, the image size $D_{\Pi'}$ in image plane Π' and the maximum sampling interval at the Nyquest sampling rate are written as

$$D_{\Pi'} = mD_\Pi, \tag{13}$$

$$\Delta D_{\Pi'} = \frac{1}{2}m\Delta = \frac{1}{2}m\frac{\mathrm{NA}}{\lambda}, \tag{14}$$

where m is the magnification of the optical microscope.

A typical example is shown in Table 1. In the calculation, the value of the field of view of a standard optical microscope having a field number of 20 has been used as the value of D_Π, the extent of the object wave. While this definition examines a critical condition, in the actual instrumentation we set the illuminated area of the object smaller than the field of view so as to ease the requirements for the pixel format and achieve a balance between the applicability of a commercially available CCD camera and the designed performance of the instrumentation.

As described in Section 4, we adopted the optical layout in which both diffraction and object intensities are measured by a single CCD camera. In this case, the requirements of Eqs. (11)–(14) must be satisfied simultaneously by a single CCD.

Table 1
Typical pixel format of CCDs required for sampling intensity data[a]

Objective[b]			Diffraction intensity		Object intensity	
NA	f (mm)	m	Image size, $D_{\Gamma'}$ (mm)	Sampling, $\Delta D_{\Gamma'}$ (μm)	Image size, $D_{\Pi'}$ (mm)	Sampling, $\Delta D_{\Pi'}$ (μm)
0.55	4.00	50	17.6	9.76	20.0	22.2
0.80	2.00	100	12.8	9.76	20.0	30.5

[a] In the calculations, wavelength was set at 488 nm and the magnification of the relay optics was set at four times. As the value of D_{Π}, the extent of the object wave (see Fig. 4), we used the value of the field of view of a standard optical microscope having a field number of 20.
[b] Nikon catalog.

3.2. Illumination system

A plane wave incident onto the object surface can be achieved using the telecentric system shown on the right-hand side of Fig. 5. A laser is used as the light source. A point source of the laser is projected onto the back focal point of the objective through two auxiliary lenses, then projected away to infinity.

In designing the illumination condition, propagation characteristics of a Gaussian beam were taken into account. First, the area of illumination on the object surface, i.e. the measurement area, was evaluated from the diameter of the beam waist of the incident Gaussian beam. (The diameter is defined by the full-width measure at which the beam intensity has fallen to $1/e^2$ of its axial value, which is denoted by $2w_0$ on the left-hand side of Fig. 5.) Second, the wavefront radius of curvature at a certain distance from the waist was considered. Because the wavefront of the incident beam is to be biased on the reconstructed phase, sufficient flatness of the incident wavefront should be kept even when illumination is defocused.

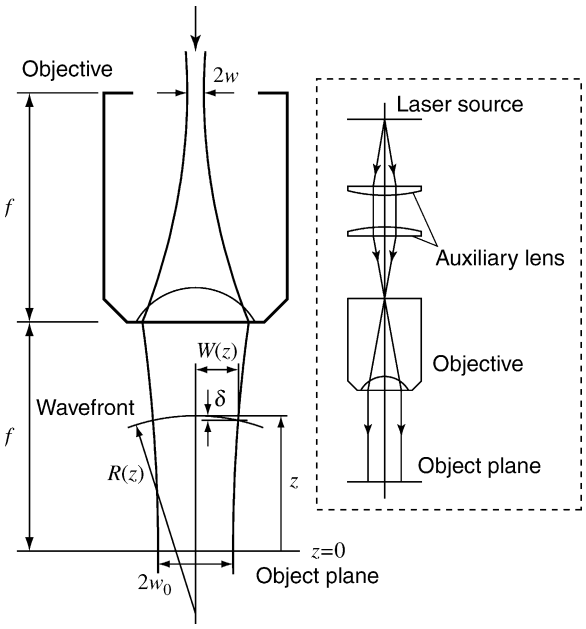

Fig. 5. Schematic of the illumination optics (right-hand side) and the calculation model used for designing the illumination condition. $2w_0$ and $2w$ are the beam diameter ($1/e^2$ full-width measure) of the incident Gaussian beam on the front and back focal planes of the objective, respectively. Wavefront error δ when illumination is defocused was evaluated using $W(z)$, $1/e$ half-width of the incident Gaussian beam at an axial distance z from the waist position, and $R(z)$, wavefront radius of curvature at an axial distance z. f is the focal length of the objective.

Table 2
Typical values calculated for illumination design[a]

Objective[b]		Waist diameter[c]	Wavefront error[d]
NA	f (mm)	$2w_0$ (μm)	δ (nm)
0.55	4.00	159.59	0.19
0.80	2.00	79.80	0.76

[a] All values were calculated with the wavelength of 488 nm.
[b] Nikon catalog.
[c] Obtained when the waist diameter $2w$ in the back focal plane of the objective (see Fig. 5) was set at 15.57 μm.
[d] Evaluated at $z = \pm 100$ μm.

We defined wavefront error δ using two parameters that describe the propagation of the Gaussian beam, as shown in Fig. 5; $W(z)$ is the $1/e$ half-width (radius), $R(z)$ is the wave-

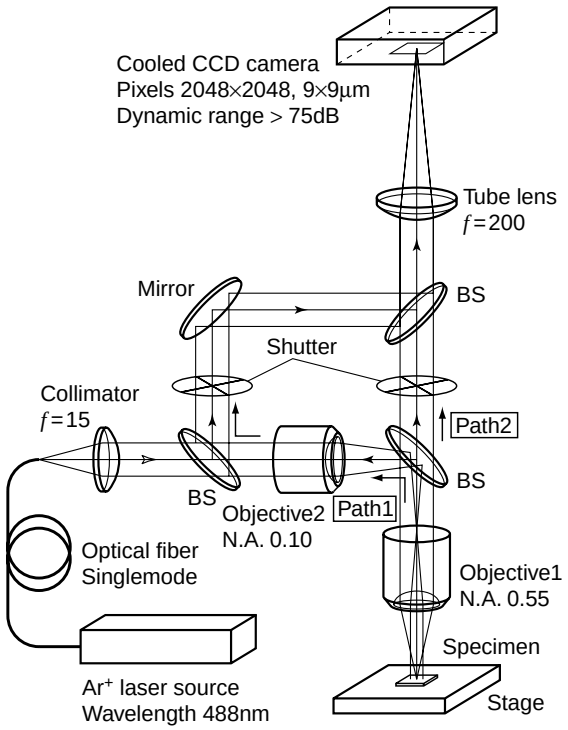

Fig. 6. Schematic illustration of the optical configuration. BS, beam splitter.

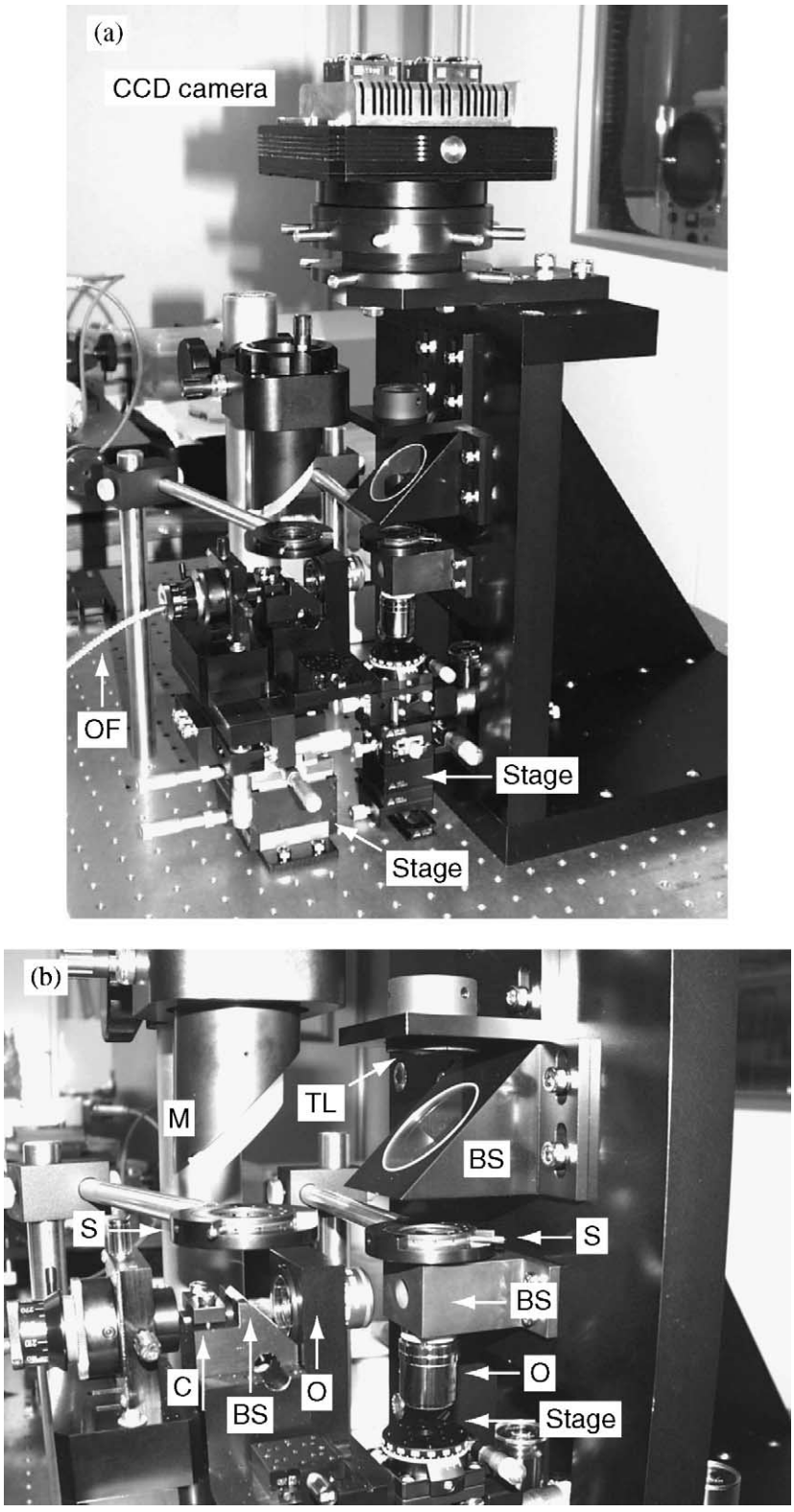

Fig. 7. Photograph of the developed instrument. (a) Instrument: OF, optical fiber. (b) Close-up view of the instrument: C, collimator; BS, beam splitter; O, objective; S, shutter; M, mirror, TL, tube lens.

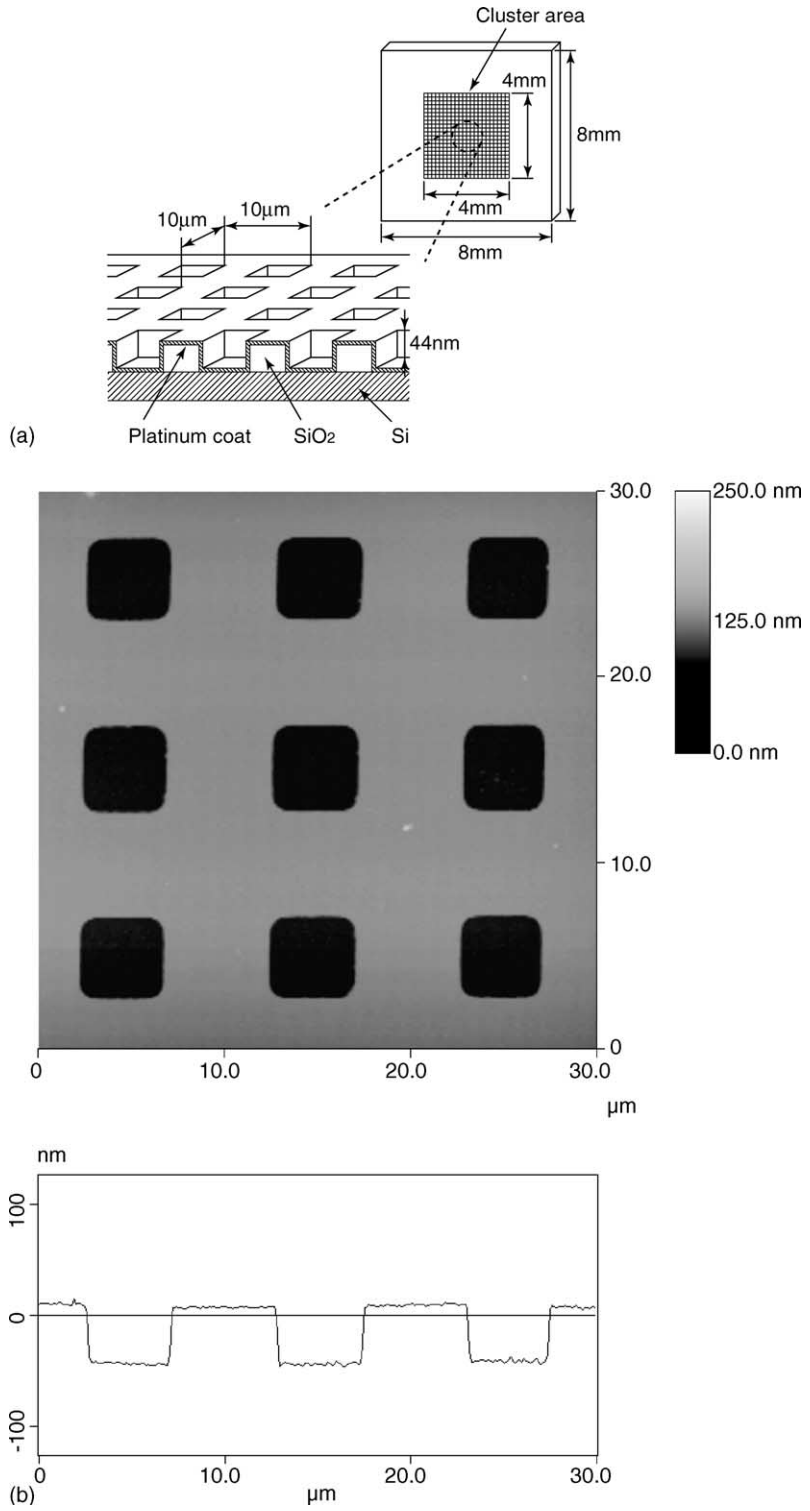

Fig. 8. (a) Sketch of the specimen. (b) Surface of the specimen obtained by atomic force microscopy (AFM).

front radius of curvature, and z is the axial distance from the waist position. These parameters are given by the following formulae [17]:

$$W(z) = w_0 \left[1 + \left(\frac{\lambda z}{\pi w_0^2} \right)^2 \right]^{1/2}, \quad (15)$$

$$R(z) = z \left[1 + \left(\frac{\pi w_0^2}{\lambda z} \right)^2 \right]. \quad (16)$$

An example of the calculated values for two different objective specifications are shown in Table 2. In the calculations, the wavelength was set at 488 nm and the error δ was evaluated at $z = \pm 100\,\mu$m. The waist diameter $2w_0$ was calculated from the beam diameter, $2w$, of 15.57 μm on the back focal plane of the objective (see Fig. 5). This value is based on the finally configured optical layout, see also Fig. 6. An illuminated area of approximately 160 μm in diameter is obtained when using the objective of NA = 0.55, and 80 μm when NA = 0.80. In both cases, the calculated values of error δ are sufficiently small for achieving vertical accuracy of nanometer. Under this illumination condition, measurements are not affected by the defocus of illumination, and hence, we require no precise positioning of the measured object. Furthermore, the large depth of focus brings about stable illumination during in-process measurements.

4. Optical instrumentation

The optical configuration of the developed instrument is shown in Fig. 6. An Ar ion laser (MELLES GRIOT 543-100BS; wavelength, 488 nm) is used as a light source, and the laser light is introduced to the instrument via a single-mode optical fiber. The collimator lens and objective2 produce a laser spot of 15.57 μm in diameter on the back focal point of objective1. With this setup, the specimen is illuminated by a Gaussian beam whose waist coincides with the specimen surface. As described in Section 3.2, there is no requirement for precise positioning of the specimen.

Light scattered from the specimen surface is gathered by objective1 (Nikon CFIC-EPI PLAN ELWD, 50×, NA of 0.55, WD of 8.70 mm), forming Fraunhofer diffraction in its back focal plane; by exchanging objective1, settings of lateral resolution, field of view and working distance can be adjusted so as to suit an individual specimen. The diffraction image is magnified four-fold by the microscope optical system consisting of objective2 (Nikon CFI PLAN, 4×, NA of 0.10, WD of 30 mm) and a tube lens, as indicated by path1 in Fig. 6. The magnified image of the specimen surface is provided by the optical microscope (path2 in the figure), which enables one to measure object intensity. A cooled CCD camera (Apogee Instruments AP4; Kodak KAF-4200; pixels, 2048 × 2048, 9 μm × 9 μm; dynamic range of >75 dB) is mounted on the instrument to measure intensity images. Two intensities are respectively measured by opening and shutting two shutters to switch the paths. The instrument was placed in a clean-room of class 5000. The developed instrument is shown in Fig. 7. The two stages indicated in Fig. 7a are used for the alignment of the specimen and of the illumination optics.

5. Experiments

Experimental verifications were performed by measuring a reference standard that was designed for characterizing SPM. Although the principles of the present method works for general three-dimensional structures, the periodic character of the standard is suitable for the first fundamental verifications of the proposed method.

5.1. Specimen

The specimen (VLSI standards STR10-440P) is illustrated in Fig. 8a. The specimen consists of an 8 mm × 8 mm silicon die with a precisely fabricated silicon dioxide pitch cluster. The cluster area is located at the center of the die and contains a grid pattern in a 4 mm × 4 mm area. The grid pattern consists of an array of alternating bars and spaces with a uniform pitch of 10 μm. The entire top surface of the die is coated with a uniform layer of platinum, and the depth of pockets is defined as 44 nm. The topography of the surface of the specimen obtained by AFM (Digital Instruments; Veeco metrology group, Nanoscope IIIa Dimension 3100) is also shown in Fig. 8b.

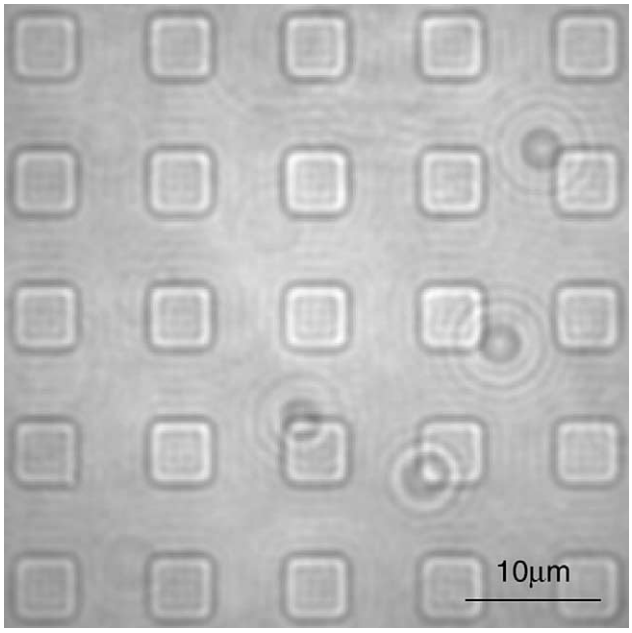

Fig. 9. Measured object intensity $i(x, y) = |V(x, y)|^2$. The obtained image was cropped and only the central part is shown.

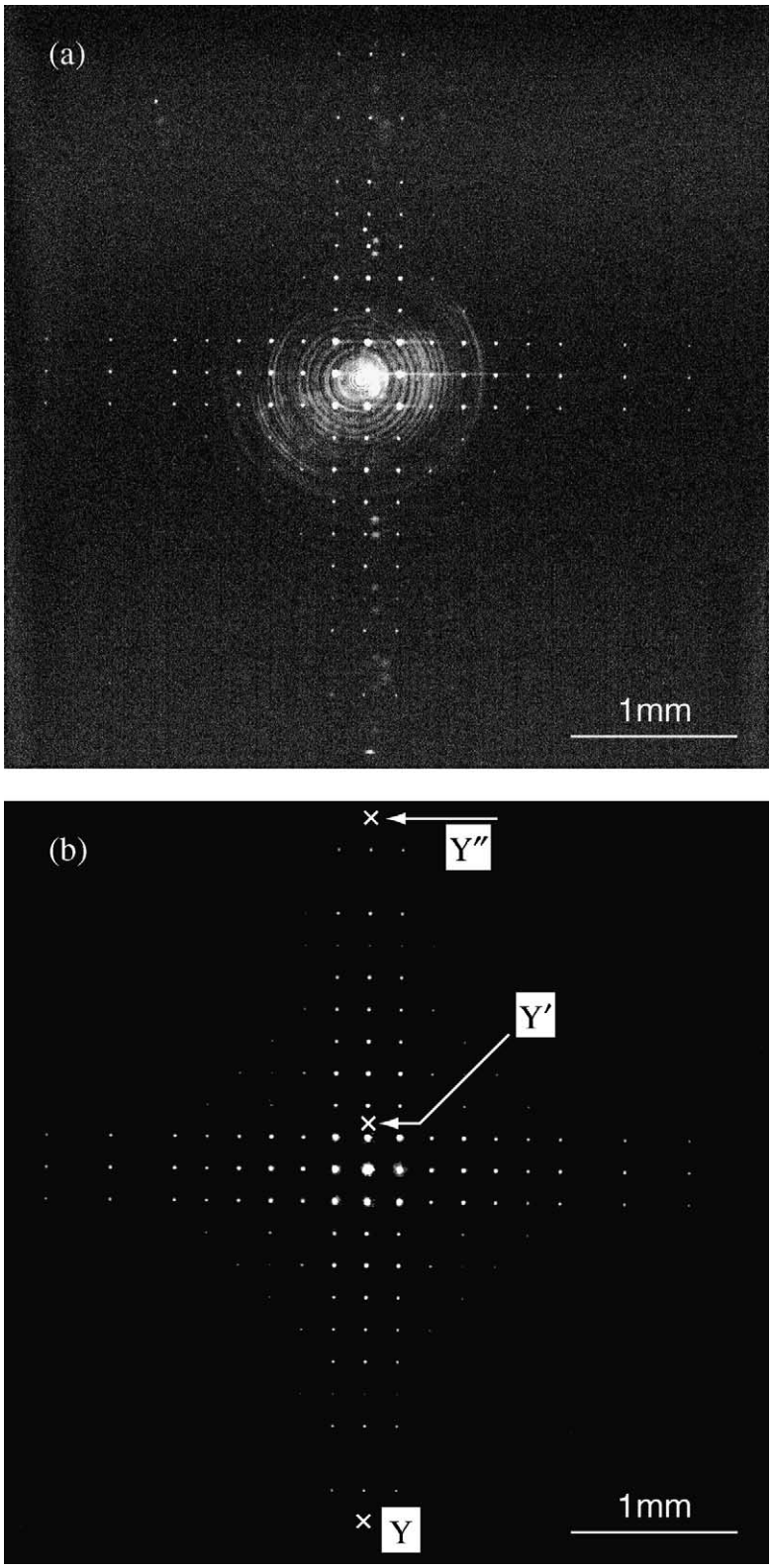

Fig. 10. Measurement of diffraction intensity $I(X, Y) = |U(X, Y)|^2$. Gray levels of the images are logarithmic. The scale bars correspond to a measurement on the back focal plane of objective1 (see Fig. 6). (a) CCD image. (b) Image of the diffraction intensity obtained after image processing.

5.2. Measurements of diffraction and object intensities

The illumination was directed to the center of the specimen. The measured diameter of the incident Gaussian beam was approximately 160 μm at its waist. Throughout the intensity measurements, bias, dark, and sensitivity variations between each pixel in the CCD chip were calibrated to improve the signal-to-noise ratio of the measured intensity values represented in the CCD images. The lateral magnifications of the imaging system were also calibrated.

The measured object intensity $i(x, y) = |V(x, y)|^2$ is shown in Fig. 9—the obtained image was cropped and only the central part is shown. A CCD image of the diffraction intensity $I(X, Y) = |U(X, Y)|^2$ is shown in Fig. 10a. Gray levels of the presented image have been stretched into the logarithmic scale. A uniform separation of each component of the Fraunhofer pattern was observed. The undesirable artifacts and measurement noise were removed by image processing techniques based mainly on image subtraction and smoothing [18]. In order to obtain sufficient signals for the high-frequency components having weak intensities, another exposure was taken with the exposure time controlled; then the two images were properly combined. Fig. 10b shows the intensity image obtained after these treatments. Measurement noise and artifacts are greatly reduced, and high-order components having weak intensity can be distinguished clearly.

The power spectrum along the line Y–Y′ in Fig. 10b is shown in Fig. 11a. Fig. 11b shows a detailed plot of the high-order spectral components [Y′–Y″ in Fig. 10b]. In these figures, spectra are normalized by the principal maximum of the zeroth-order component. Spectra up to the tenth order could be obtained, distributed over a dynamic range of more than 100 dB. Each successive spectrum is uniformly separated by $10^5\,\mathrm{m}^{-1}$, i.e. the reciprocal of the nominal pitch of the specimen.

5.3. Surface reconstruction results and discussion

An ideal surface profile corresponding to the nominal dimensions of the specimens was used as the initial phase estimate of the algorithm, then 300 iterations followed. A curve of normalized rms error E_k^2 against the number of iterations is shown in Fig. 12. After the rapid decrease within the initial few iterations, the value of the normalized rms error decreased to approximately 0.04.

The surface profile calculated from the reconstructed phase using Eq. (2) is shown in Fig. 13a and b; Fig. 13b is a magnified plot of area Σ in Fig. 13a. Each rectangular pocket having the width of 5 μm is clearly distinguished. In Fig. 13a, a circle having the diameter of the incident Gaussian beam, 160 μm, has been drawn. Shapes of each pocket were uniformly reconstructed inside the circle, while outside the circle, the reconstructed profile was distorted. This indicates the measurement area can be considered to be consistent with the beam diameter of the incident Gaussian beam.

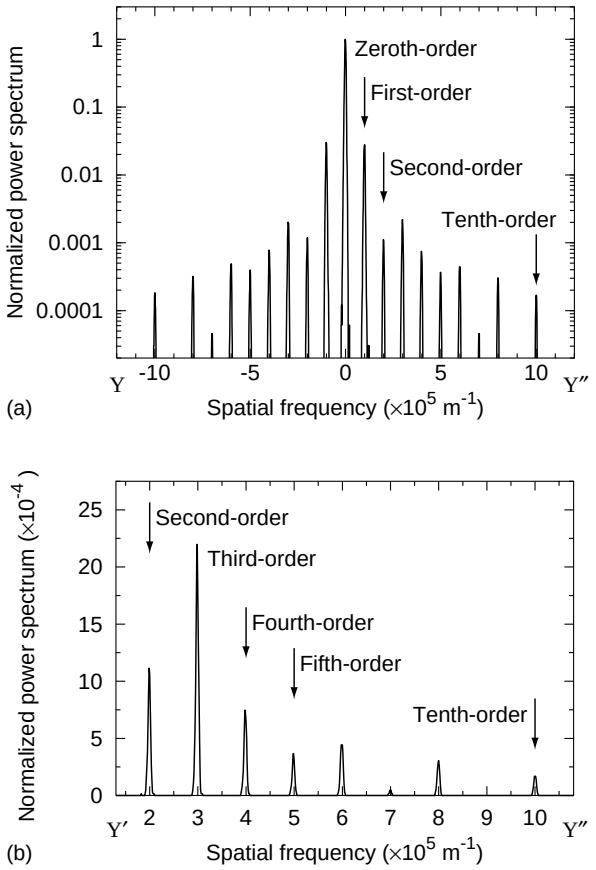

Fig. 11. Plot of power spectrum calculated from the measured diffraction intensity. The spectrum is normalized by the principal maximum of the zeroth-order component. (a) Line plot along Y–Y″ in Fig. 10b. (b) Detailed plot of the high-order spectral components [Y′–Y″ in Fig. 10b].

The surface of area Σ' and the section profile along line X–X′ in Fig. 13b are shown in Fig. 14a and b, respectively. The dimensions of the measured profile are in good agreement with the nominal values of the specimen: pitch of 10 μm and depth of 44 nm. As indicated in Fig. 14b, the lateral resolution experimentally obtained from the slope at the side wall of the pockets was well reproduced by the theoretically predicted value given by Eq. (10), $\lambda/\mathrm{NA} = 0.89\,\mu\mathrm{m}$.

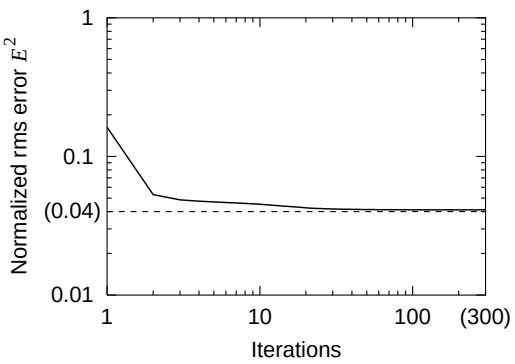

Fig. 12. Iterations vs. normalized rms error.

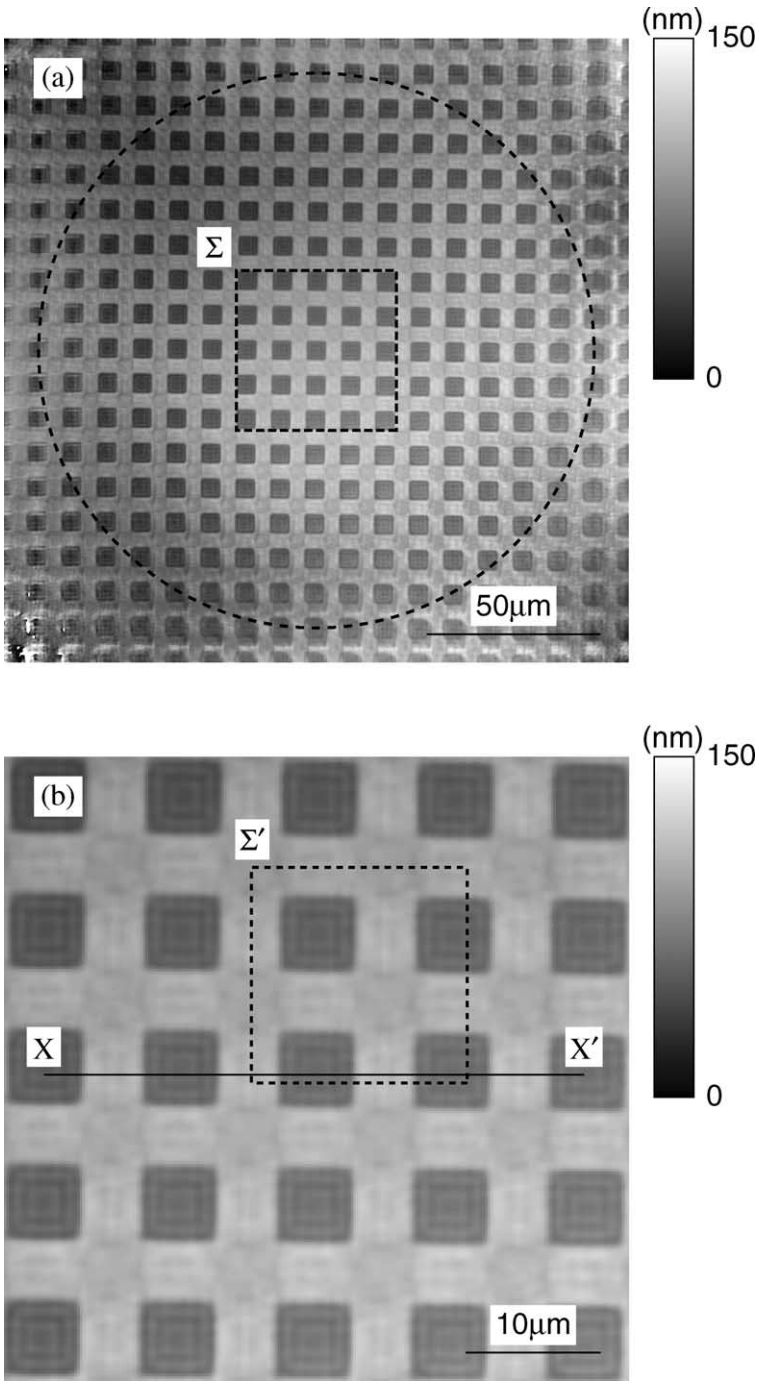

Fig. 13. (a) Surface reconstructed by phase retrieval. Surface height is represented by gray level. Diameter of the dashed circle corresponds to the diameter of the incident Gaussian beam, 160 μm. (b) Magnified plot of area Σ in (a).

The measured profile is slightly wavy, having, at most, ±5 nm deviation in its height when compared with the one obtained by AFM [see also Fig. 8b]. The wavy character is attributed to a physical property inherent to coherent imaging. In coherent imaging, the measured spectrum suddenly drops to zero outside the bandwidth of the system. This brings about Gibbs phenomenon [19] in the reconstructed profile (ringing effect). Noise in the intensity measurements can also be counted as other causes of the deviation. Systematic error, such as imperfections of the CCD chip and lens aberrations of the imaging system, can be compensated to improve the accuracy of the reconstructed profile; the majority of the CCD-oriented problems can be eliminated by performing more careful calibrations of the CCD chip, while the error caused by lens aberrations can be deconvolved on the basis of the optical transfer function (OTF) of the present imaging system.

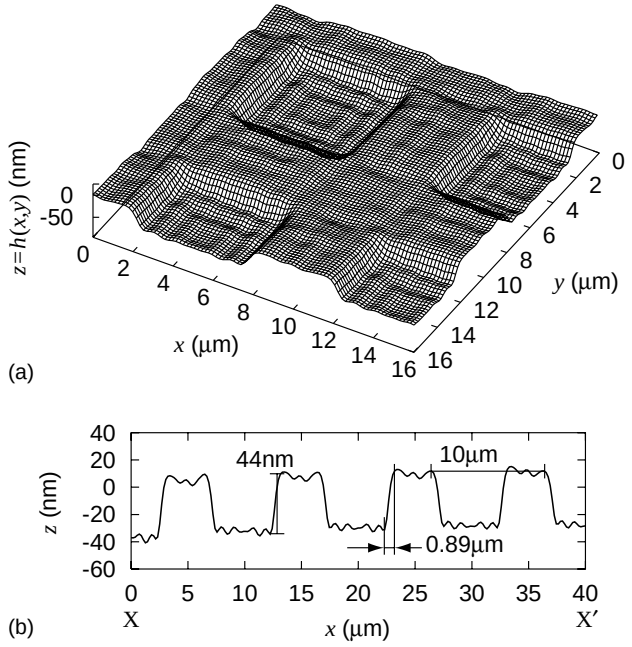

Fig. 14. (a) Surface plot of area Σ' in Fig. 13b. (b) Section profile along line X–X′ in Fig. 13b.

6. Conclusions

We proposed an optical profiler based on the phase retrieval technique. In the present method, the power spectrum of the microsurface profile is obtained by measuring the Fraunhofer diffraction intensity. With the additionally measured object intensity, the surface profile is deterministically reconstructed from the obtained power spectrum, by using phase retrieval.

We also designed an optical instrument on the basis of the measurement principles proposed. Illumination conditions and the sampling requirements were examined to prepare a practical design. Using the developed instrument, we measured the surface of a reference standard having rectangular pockets 44 nm deep at intervals of 10 μm. It was demonstrated that a surface profile is successfully reconstructed within the area inside the $1/e^2$ full-width of the incident Gaussian beam. The dimensions of the measured surface were consistent with the nominal values of the specimen. Good agreement between the surface profile obtained by the present method and that obtained by AFM was also observed with, at most, ±5 nm deviation in height. These experimental results support the validity of the instrumentation as well as the measurement principles.

The present method is suitable for applications to in-process or near-process and on-machine measurements of microsurface profiles in a production environment. Application to the measurement of non-periodic surfaces will be done in future work.

Acknowledgments

This study is partly supported by the JSPS Research Fellowships for Young Scientists (#01145). We would like to thank K. Yamashita and H. Yamakita for their assistance.

References

[1] Nagel DJ, Zaghloul ME. MEMS: micro technology, mega impact. IEEE Circuits Dev Mag 2001;17(2):14–25.
[2] Pfeifer T, Freudenberg R, Dussler G, Bröcher B. Quality control and process observation for the micro assembly process. Measurement 2001;30:1–18.
[3] Luke DR, Burke JV, Lyon RG. Optical wavefront reconstruction: theory and numerical methods. SIAM Rev 2002;44(2):169–224.
[4] Gerchberg RW, Saxton WO. A practical algorithm for the determination of phase from image and diffraction plane pictures. Optik 1972;35(2):237–46.
[5] Fienup JR. Phase retrieval algorithms: a comparison. Appl Opt 1982;21(15):2758–69.
[6] Beckmann P, Spizzichino A. The scattering of electromagnetic waves from rough surfaces. Norwood, MA: Artech House; 1987.
[7] Vorburger TV, Marx E, Lettieri TR. Regimes of surface roughness measurable with light scattering. Appl Opt 1993;32(19):3401–8.
[8] Valliant JG, Feloy MP, Bennett JM. Instrument for on-line monitoring of surface roughness of machined surfaces. Opt Eng 2000;39(12):3247–54.
[9] Hertzsch A, Kröger K, Truckenbrodt H. Microtopographic analysis of turned surfaces by model-based scatterometry. Precision Eng 2002;26(3):306–13.
[10] Destouches N, Guérin CA, Lequime M, Giovannini H. Determination of the phase of the diffracted field in the optical domain—application to the reconstruction of surface profiles. Opt Commun 2001;198:233–9.
[11] Miyoshi T, Takaya Y, Saito K. Micromachined profile measurement by means of optical inverse scattering phase method. Ann CIRP 1996;45(1):497–500.
[12] Fienup JR. Reconstruction of an object from the modulus of its Fourier transform. Opt Lett 1978;3(1):27–9.
[13] Fienup JR. Reconstruction of a complex-valued object from the modulus of its Fourier transform using a support constraint. J Opt Soc Am A 1987;4(1):118–23.
[14] Taguchi A, Miyoshi T, Takaya Y, Takahashi S, Saito K. 3D micro-profile measurement using optical inverse scattering phase method. Ann CIRP 2000;49(1):423–6.
[15] Born M, Wolf E. Principles of optics. New York: Pergamon Press; 1980.
[16] Brigham EO. The fast Fourier transform. Englewood Cliffs, NJ: Prentice-Hall; 1974.
[17] Siegman AE. An introduction to lasers and masers. New York: McGraw-Hill; 1971.
[18] Kawata S, Minami S. Adaptive smoothing of spectroscopic data by a linear mean-square estimation. Appl Spectrosc 1984;38:49–58.
[19] Papoulis A. The Fourier integral and its applications. New York: McGraw-Hill; 1962.